Transparent, Superhydrophobic Surfaces from One-Step Spin Coating of Hydrophobic Nanoparticles

ARTICLE *in* ACS APPLIED MATERIALS & INTERFACES · FEBRUARY 2012

Impact Factor: 6.72 · DOI: 10.1021/am201750h · Source: PubMed

4 AUTHORS, INCLUDING:

Lebo Xu
WestRock
8 PUBLICATIONS **209** CITATIONS
SEE PROFILE

Shu Yang
University of Pennsylvania
207 PUBLICATIONS **5,156** CITATIONS
SEE PROFILE

ACS APPLIED MATERIALS & INTERFACES

Research Article

www.acsami.org

Transparent, Superhydrophobic Surfaces from One-Step Spin Coating of Hydrophobic Nanoparticles

Lebo Xu,[†] Raghuraman G. Karunakaran,[†] Jia Guo, and Shu Yang*

Department of Materials Science and Engineering, University of Pennsylvania, 3231 Walnut Street, Philadelphia, Pennsylvania 19104, United States

Supporting Information

ABSTRACT: We study the nonwettability and transparency from the assembly of fluorosilane modified silica nanoparticles (F-SiO_2 NPs) via one-step spin-coating and dip-coating without any surface postpassivation steps. When spin-coating the hydrophobic NPs (100 nm in diameter) at a concentration ≥0.8 wt % in a fluorinated solvent, the surface exhibited superhydrophobicity with an advancing water contact angle greater than 150° and a water droplet (5 μL) roll-off angle less than 5°. In comparison, superhydrophobicity was not achieved by dip-coating the same hydrophobic NPs. Scanning electron microscopy (SEM) and atomic force microscopy (AFM) images revealed that NPs formed a nearly close-packed assembly in the superhydrophobic films, which effectively minimized the exposure of the underlying substrate while offering sufficiently trapped air pockets. In the dip-coated films, however, the surface coverage was rather random and incomplete. Therefore, the underlying substrate was exposed and water was able to impregnate between the NPs, leading to smaller water contact angle and larger water contact angle hysteresis. The spin-coated superhydrophobic film was also highly transparent with greater than 95% transmittance in the visible region. Further, we demonstrated that the one-step coating strategy could be extended to different polymeric substrates, including poly(methyl methacrylate) and polyester fabrics, to achieve superhydrophobicity.

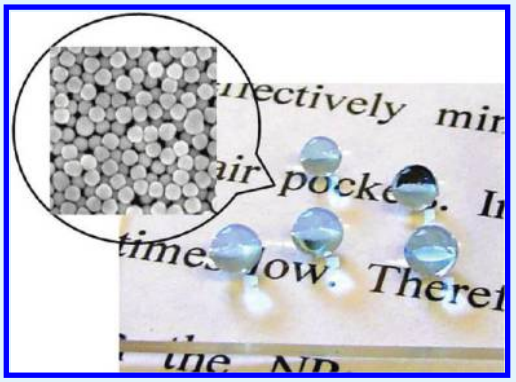

KEYWORDS: *superhydrophobic surfaces, transparent, silica nanoparticles, spin coating, nanoroughness, close-packed assembly*

INTRODUCTION

Superhydrophobic surface with a water contact angle of 150° or higher and very little flow resistance are of interest for numerous applications, including self-cleaning coatings, impermeable textiles, microfluidics, lab-on-a-chip devices, and biotechnology. To create superhydrophobic surface, a combination of low surface energy chemistry and dual-scaled (micro and nano) surface roughness is needed. There has been significant progress both theoretically[1−4] and experimentally in creating topographically rough surfaces with extremely high water-repellency.[1,5−14] Recently, there have been increasing interest in energy efficient coatings that are both self-cleaning and transparent for potential applications, such as solar cells, window treatment, and optical equipment.

Transparency and surface roughness are generally competitive properties. When surface roughness increases, hydrophobicity increases, whereas the transparency often decreases because of Mie scattering from the rough surface. When the roughness dimension is much smaller than the light wavelength, the film becomes increasingly transparent due to refractive index change between air and substrate, which effectively reduces the intensity of refraction at the air (or water)/film interface and increases the optical quality. To achieve high transparency in the visible light, the size of surface roughness should be no larger than 100 nm. A few groups have attempted to create transparent superhydrophobic surfaces.[8,15−25] Often times, the fabrication either requires expensive lithographic tools to achieve small feature size, or involves rather complicated chemical synthesis procedures. Recently, highly transparent superhydrophobic surface has been demonstrated by dip-coating either a single layer of 60 nm SiO_2 nanoparticles (NPs)[26] or dual-sized SiO_2 NPs (100 and 15 nm sequentially)[27] onto different substrates, followed by perfluorosilane deposition.

Compared to the synthesis of porous hydrophobic polymer films and the use of other NPs (e.g., TiO_2 and ZnO) and nanowires, silica NPs offer benefits of simplicity, low cost, tunable size, and excellent scratch resistance. However, they are typically hydrophilic and negatively charged. To make a surface superhydrophobic using silica NPs, a thin layer of low-surface-energy coating is necessary to be deposited on the newly generated rough surface, which is usually achieved by vapor deposition under vacuum or by solution casting. However, the post-treatment step could significantly increase the cost of coating for large-area substrates, and may not be desirable for certain polymeric substrates or applications in consumer

Received: December 10, 2011
Accepted: January 16, 2012
Published: January 31, 2012

products. It remains intriguing whether it is possible to eliminate the postpassivation step but still achieve superhydrophobicity and high transparency from the assembly of hydrophobic NPs (size ≤100 nm). It requires control of the hydrophobic NP's coverage on the surface to minimize the exposure of the underlying substrate, which may not be hydrophobic.

In this report, we studied the nonwettability and transparency of assembled fluorosilane modified silica (F-SiO_2) NPs (100 nm in diameter). When the F-SiO_2 NPs (≥0.8 wt % in a fluorinated solvent) were spin coated on various substrates (hydrophilic, hydrophobic Si and polymers), the surface exhibited superhydrophobicity, which was not achieved by dip-coating method. Scanning electron microscopy (SEM) and atomic force microscopy (AFM) images revealed that F-SiO_2 NPs were nearly close-packed in the spin coated, superhydrophobic films, but randomly distributed in the dip coated films. The superhydrophobic coating was found highly transparent. UV−vis spectra showed greater than 95% transmittance in the visible region.

EXPERIMENTAL SECTION

Materials. All chemicals were used as received. 3-(triethoxysilyl)-propyl succinic anhydride (TESPSA) (95%), (heptadecafluoro-1,1,2,2,-tetrahydrodecyl)trichlorosilane (99%), namely F-silane, and (heptadecafluoro-1,1,2,2,-tetrahydrodecyl) dimethylchlorosilane (HDFTHD) (99%) were purchased from Gelest, Inc. Triethylamine (99%), toluene (anhydrous), and decafluoropentane (60%) were purchased from Sigma Aldrich. Si wafer (P type, polished) was purchased from Siltron Inc. (Korea). Silica NPs (100 ± 3 nm, 30 wt % in isopropanol) were provided by Nissan Chemicals (Houston, TX, USA). The fluorinated solvent, Novec 7300 was provided by 3 M (St. Paul, MN, USA). Polyester fabric was provided by Bigsky Technologies (Pittsford, New York, USA).

Surface Treatment of Silicon Substrates. The Si wafers were precleaned using 1% solution (*v*/*v*) of Detergent 8 (a low foaming phosphate free cleaner soap solution from Alconox) in deionized (DI) water at 65 °C for 1 h, followed by sonication in DI water, isopropanol and acetone for 20 min, respectively. After drying, the substrates were treated with oxygen plasma (30 W, 0.2 Torr, Harrick plasma cleaner PDC-001) for 1 h. The oxidized Si wafers were then silanized immediately by immersing them in 0.01 M TESPSA in anhydrous toluene overnight. The physisorbed silane was removed by sonicating in ethanol and acetone for 30 min, respectively, followed by drying with compressed air. The fluorosilane treatment on Si wafers was done by vapor deposition of F-silane for 1 h onto oxidized Si wafers in vacuo.

Surface Functionalization of Silica Nanoparticles with Fluorosilane. The as-received silica NPs were pelletized by centrifugation at 11 000 rpm overnight, followed by drying under vacuum for 3 h. The NPs were then functionalized with HDFTHD using triethyl amine (TEA) as an acid scavenger.[28] In a typical experiment, 5.0 g silica NPs were dispersed in 50 mL of toluene. 1 mL TEA was added to this NP dispersion under nitrogen atmosphere. Then 5 mL 0.01 M HDFTHD/toluene solution was added to the NPs suspension and allowed to react at room temperature for at least 18 h (Figure 1). Once the NP surface was functionalized with sufficient amount of HDFTHD, it started to precipitate along with TEA salts. The fluorofunctionalized silica NPs (F-SiO_2 NPs) were purified via centrifugation at 6000 rpm for 3 h, followed by repeated washing with acidified water, water, ethanol, and toluene, respectively, to remove TEA salts and unreacted and partially functionalized silica NPs. Additional centrifugation could be performed if necessary. Finally, the F-SiO_2 NPs were dried under a vacuum for 3 h.

Preparation of Nanoparticle Films. For spin-coating, the F-SiO_2 NPs were dispersed in Novec 7300 at different weight percentages and sonicated for 30 min prior use. They were then spin coated at 1500 rpm for 20 s at a velocity of 150 rpm/s onto TESPSA treated Si wafers. For dip-coating of F-SiO_2 NPs, the silanized Si wafers were immersed into a decafluoropentane solution of well-dispersed F-SiO_2 NPs with different concentrations for 10 s and withdrawn at a rate of 4 cm/min.

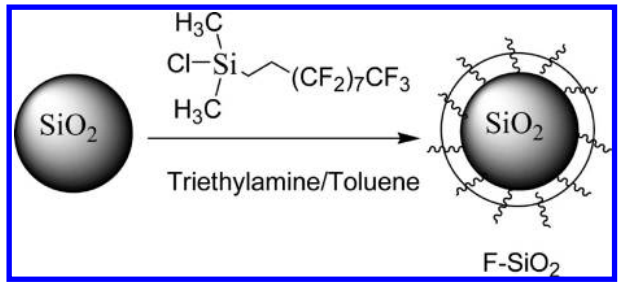

Figure 1. Schematic illustration of the synthesis of fluorosilane coated silica nanoparticle, F-SiO_2 NP.

Water Drop Test and Scotch Tape Test. In water drop test, about 1000 water droplets (ca. 80 μL) were dropped from about 1 ft above the sample. Afterward, the water contact angle was measured on the sample. In Scoth tape test, a pressure was applied to ensure good contact between the tape and the NP coating, followed by peeling off the tape. The DI water contact angles and AFM images were collected on samples before and after the tests.

Characterization. The water contact angles were measured by Ramé-Hart standard automated goniometer (Model 290). The static contact angle was measured from a 5 μL DI water droplet. Advancing and receding water contact angles were measured by adding and removing water from the substrate, respectively. For roll-off angle measurement, the substrate was placed on a custom-designed stage with protractor attached to it and a 5 μL water droplet was used. All water contact angle and roll-off angle values were averaged over three measurements on different areas of each sample. The morphologies of the NP films, which were sputter-coated with gold, were imaged by FEI Quanta 600 FEG Environmental Scanning Electron Microscopy (ESEM). The surface topography of the samples was imaged by Dimension 3000 Atomic Force Microscopy (Digital Instruments), with a Si_3N_4 cantilever in tapping mode. The root-mean-square (rms) roughness values were calculated from 5 μm × 5 μm images using nanoscope VII software. The optical transparency of the nanoparticle coated glass substrates was measured using a Varian UV−vis−NIR Cary 5000 spectrophotometer. Blank glass was used as reference.

RESULTS AND DISCUSSION

The wetting behavior of a surface is dependent on both surface chemistry and surface topography. There are two distinct models by Wenzel[29] and Cassie−Baxter.[30] In Wenzel's model, roughness effectively increases the actual surface area. The apparent Wenzel contact angle, θ^w, on a rough surface is defined as

$$\cos \theta^w = r \cos \theta_0 \quad (1)$$

where r is the roughness factor and defined as the ratio of actual surface area over the apparent surface area, and θ_0 is the equilibrium contact angle on a flat surface or the Young's contact angle. On a hydrophobic surface ($\theta_0 > 90°$), θ^w is increased by roughness. When the substrate is intrinsically hydrophilic ($\theta_0 < 90°$), solid−liquid interaction is favored; θ^w will be decreased by roughness, resulting in spontaneous spreading on the rough surface. In the Cassie−Baxter model, it is considered that liquid contacts a heterogeneous surface, and the apparent contact angle, θ^c, can be described as

$$\cos \theta^c = f_1 \cos \theta_1 + f_2 \cos \theta_2 \quad (2)$$

Table 1. Water Contact Angles of Spin-Coated and Dip-Coated 100 nm F-SiO_2 NPs on Different Substrates at Various NP Concentrations

sample	coating method	[NPs] (wt%)	surface pretreatment	θ_{adv} (deg)	θ_{rec} (deg)	$\Delta_\theta = \theta_{adv} - \theta_{rec}$ (deg)
control			TESPSA	37.1 ± 2	27.9 ± 1	9.2 ± 2
control			F-silane	113.4 ± 1	110.5 ± 2	2.9 ± 2
control			DHFTHD	112.8 ± 1	111.2 ± 1	1.6 ± 1
1	spin	0.1	TESPSA	129.3 ± 4	77.8 ± 6	51.5 ± 7
2	spin	0.4	TESPSA	151.0 ± 1	113.0 ± 1	38.0 ± 1
3	spin	0.8	TESPSA	160.4 ± 2	N/A[a]	
4	spin	1	TESPSA	156.0 ± 3	N/A[a]	
5	spin	1.2	TESPSA	159.2 ± 1	N/A[a]	
6	dip	0.8	TESPSA	88.9 ± 2	58.2 ± 1	30.7 ± 2
7	dip	0.8	F-silane	141.0 ± 1	134.1 ± 1	6.9 ± 1

[a]the water contact angle not measurable because of the high mobility of water droplet.

where f_1 and f_2 are fraction of different surface components ($f_1 + f_2 = 1$), θ_1 and θ_2 are Young's contact on the homogeneous surface of each components respectively. When air is trapped in the grooves of the rough surface, the surface is considered to be a composite surface of solid and air, and eq 2 becomes

$$\cos\theta^c = f(\cos\theta_0 + 1) - 1 \quad (3)$$

where f is the fraction of liquid−solid contact. θ^c increases with decreasing f as more air is trapped between the grooves of the rough surface. To achieve superhydrophobicity, dual-scale roughness is often required together with an intrinsic hydrophobic nature of the substrate.,[1,5−1327]

Two general strategies have been used to create a superhydrophobic surface: (1) introduction of surface roughness or porosity on a low surface energy material, and (2) creation of roughness on surface, followed by deposition of a low surface energy material on top of it. The first approach does not require post-treatment of the substrate; however, the procedure of creating roughness from a low surface energy material is often specialized and complicated. The second approach is simple, low-cost, and versatile, for example, using nanoparticle assemblies. However, a post-treatment of the rough surface with a thin layer of hydrophobic coating is essential, especially if the original substrate is not hydrophobic. The deposition of low-surface-energy coating will prevent the exposure of hydrophilic regions, and thus modify the liquid−solid surface interface. However, this post-treatment may not be desirable for large panel coatings or consumer-friendly products.

Previously, we obtained optically transparent, superhydrophobic surfaces by the deposition of aminosilane functionalized silica NPs of two different sizes, followed by perfluorosilane treatment.[27] Like many other literature reported to create transparent superhydrophoibicity, it requires a multistep process, including substrate surface pretreatment, sequential assembly of NPs with different sizes for suitable roughness, followed by heating to induce covalent bonding between NPs and substrate, and last vapor deposition of a hydrophobic passivation layer on NPs. However, vacuum deposition in the last step will significantly increase the cost of coating large-area substrates, and may not be desirable for coating certain polymeric substrates, nor it is accessible to general consumers who will apply the coatings themselves. In this study, we exploit the possibility of a low-cost and simple solution to create superhydrophobic surface from one-step assembly of single-sized NPs on both hydrophilic and hydrophobic substrates without surface post-treatment. In this regard, surface hydrophobilization of the silica NPs and control of their surface coverage on the substrate are investigated.

The synthesis of fluorosilane functionalized silica NPs is depicted in Figure 1 by reacting the hydrophilic silica NPs with (heptadecafluoro-1,1,2,2,-tetrahydrodecyl) dimethylchlorosilane (HDFTHD). It is important to perform multistep washing and centrifugation to ensure complete removal of the unreacted and partially functionalized silica NPs, which would otherwise become pinning sites of the water molecules in the later wetting studies. The obtained F-SiO_2 NPs could form stable dispersion only in fluorinated solvents. Thus, Novec 7300 and decafluoropentane were used for spin-casting and dip-coating, respectively.

Because one of our primary aims here is to eliminate the post-treatment, it is important to control the surface coverage of the hydrophobic NPs to minimize exposure of the underlying substrate, especially when the substrate is relatively hydrophilic. It is demonstrated that silica NPs dip-coated on a flat substrate are random and non-close-packed,[26,27,31,32] whereas spin-coating could lead to close-packed colloidal crystals due to shear-induced ordering.[33,34] Therefore, to pursue high surface coverage, it may be desirable to spin coat the NPs. It remains unclear whether the close-packed hydrophobic NPs themselves will offer superhydrophobicity considering that the solid filling fraction, f, is high. Previously, water repellency has been shown on the surface of nonclose packed polystyrene beads[11] after plasma etching to reduce the bead size (decreasing f), and on the inverse microporous opal.[35,36] Nevertheless, coating a thin hydrophobic layer on the etched beads or the porous structures is essential to achieve superhydrophobicity.

We employed 100 nm F-SiO_2 NPs for dip-coating and spin-coating, and varied their concentrations in fluorinated solvents. TESPSA treated Si wafers were used as substrates, which were relatively hydrophilic compared to F-SiO_2 NPs, to investigate the effect of surface coverage on the wetting behavior. First, we spin-coated F-SiO_2 NPs (samples 1 to 5), and the dynamic water contact angles on coated Si substrates are summarized in Table 1.

Increase of water contact angle and decrease of contact angle hysteresis were observed on spin-coated films when the NPs concentration was increased, suggesting a transition from Wenzel state to Cassie−Baxter nonwetting state. When the concentration of F-SiO_2 NP was increased to ≥0.8 wt %, the spin-coated surface became superhydrohpobic with an advancing water contact angle >150° and the receding contact angle was not measurable due to high mobility of the water

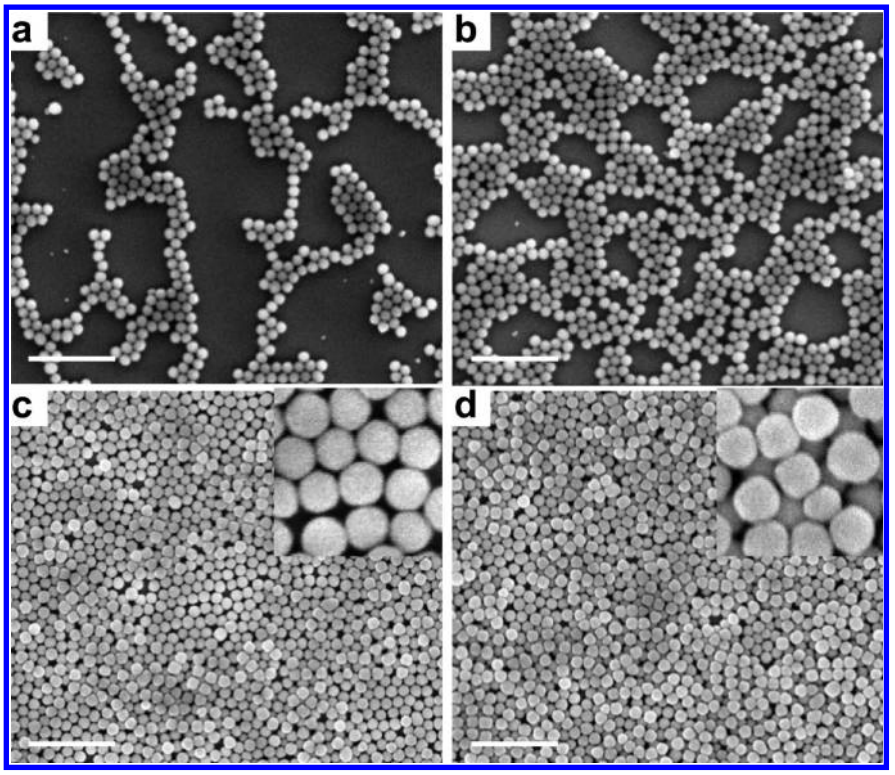

Figure 2. SEM images of spin-coated 100 nm F-SiO_2 NPs with different concentrations on TESPSA-functionalized Si wafers: (a) 0.1, (b) 0.4, (c) 0.8, and (d) 1.2 wt %. The insets in c and d are high-magnification images. Scale bars: 1 μm.

droplets. SEM images (see Figure 2) revealed that when increasing NP concentration, the NP assembly changed from random, nonclose packed (0.1 wt % and 0.4 wt %) to nearly close-packed (≥0.8 wt %), by which the substrate was fully covered. In addition, the 0.8 wt % NP film had a few second layer NPs covered on top of the first layer, whereas 1.2 wt % NP film appeared to have much more double-layered NPs (see Figure 2c, d).

The surface topography of the spin-coated NP films was investigated by AFM (Figure 3). The surface coverage indicated by AFM images agrees with that from SEM images very well. In addition, AFM images suggest that the surface roughness, rms, decreases when increasing the NP coverage on surface, from 51.20 nm (0.1 wt %) to 49.70 nm (0.4 wt %) to 25.80 nm (0.8 wt %) to 13.90 nm (1.2 wt %).

The roughness factor, r, can be estimated from AFM data to predict the Wenzel water contact angle as summarized in Table 2. When the concentration of NPs was greater than 0.4 wt %, surface was almost covered by F-SiO_2 NPs. In this case, the theoretical Wenzel contact angle, θ^w, can be estimated using the water contact angle on F-silane SAM as θ_0 in eq 1.

By comparing the measured θ_{st} and theoretical Wenzel angle, θ^w, one can see that when NP concentration is 0.4 wt %, the measured value is close to the predicted Wenzel contact angle. When NPs concentration was greater than 0.4 wt %, the measured contact angle was much higher than the predicted Wenzel contact angle, suggesting that water did not penetrate grooves between NPs, that is, Cassie−Baxter nonwetting behavior as shown in Figure 4.

To confirm this, we estimated the azimuthal angle, ø (see Figure 4), representing the level of water wetting on the particle surface. By assuming that the wetting line holds at the same level and the liquid penetration between particles can be ignored, the filling fraction can be expressed as[31]

$$f = \frac{2\pi R^2(1 - \cos\varphi)N}{2\pi R^2(1 - \cos\varphi)N + (1 - \pi(R\sin\varphi)^2 N)} \quad (4)$$

where R is the radius of nanoparticles in average (~65 nm), N is the number density of nanoparticles (see Table 2). R and N were measured from AFM images. For samples with [NPs] = 0.8 wt % and 1.2 wt %, we calculated f using Cassie−Baxter model, eq 3. Then, using eq 4, we obtained the ø as 28.5° and 29.9°, respectively. The results indicate the water merely wets the top area of NPs, in agreement with the Cassie−Baxter nonwetting behavior from the close-packed F-SiO_2 NP films.

The surface morphologies of NP coatings at different concentrations revealed by SEM and AFM images corroborate with the water contact angle results. At low NP concentration, NPs were not able to cover the underlying substrate. Because TESPSA-treated Si is hydrophilic with a static water contact angle of 36.2 ± 1°, from eq 2, we can see that large fraction of exposed TESPSA surface, f_1, will lead to wettable surface (with large contact angle hysteresis), even if it has relatively large water contact angle. When gradually decreasing f_1 and increasing f_2 (fraction of hydrophobic F-SiO_2 NP), the water contact angle increased while the contact angle hysteresis decreased. When the surface was completely covered by the F-SiO_2 NP, the surface became Cassie−Baxter nonwettable surface with air pocket trapped in-between F-SiO_2 NPs (concentration ≥0.8 wt %) and the water contact angle should be described by eq 3. According to eq 3, increasing f will decrease the apparent water CA. In Table 1, we did observe slight decrease of the apparent water CA in samples 3, 4, and 5 when increasing the NP concentration, although the NP films remained superhydrophobic. However, at NP concentration ≥0.8 wt %, their assembly became close-packed. Further

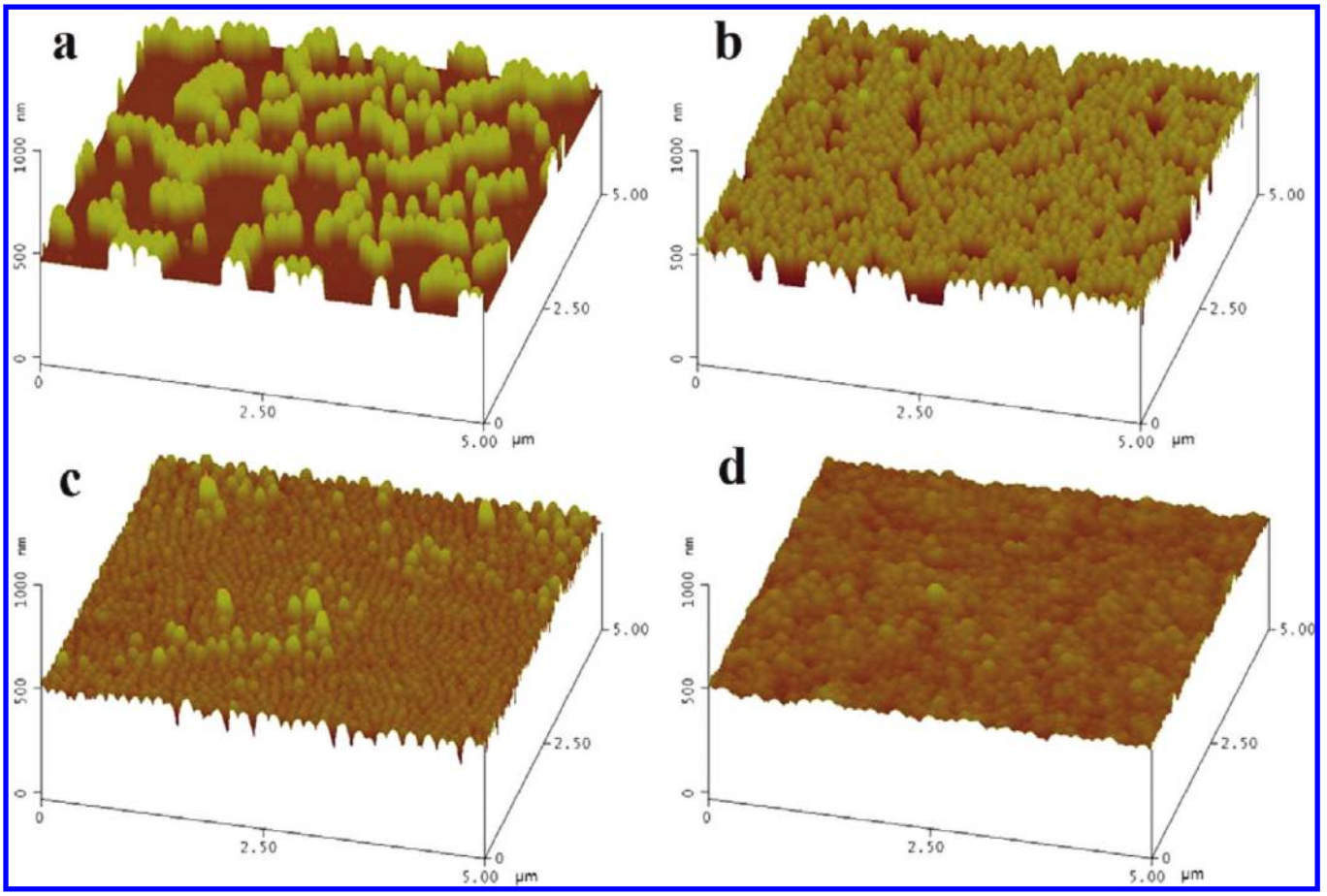

Figure 3. AFM images of 100 nm F-SiO_2 NPs spin-coated on TESPSA treated Si wafers from Novec 7300 solutions at different NP concentrations: (a) 0.1, (b) 0.4, (c) 0.8, and (d) 1.2 wt %.

Table 2. Measured Static Water Contact Angle (θ_{st}), Roughness Factor (r), Number Density of Nanoparticles (N), Theoretical Wenzel Contact angle (θ^w), Filling Fraction (f), and Estimated Azimuthal Angle (ω)

sample	θ_{st} (°)	r	N (per m^2)	θ^w (deg)	f	ø (°)
F-silane SAM	113.0	1.00		113.0		
0.4 wt % coating	137.1	1.80	5.05×10^{13}	134.7		
0.8 wt % coating	149.7	1.54	7.10×10^{13}	127.0	0.23	28.5
1.2 wt % coating	147.3	1.31	7.48×10^{13}	120.8	0.26	29.9

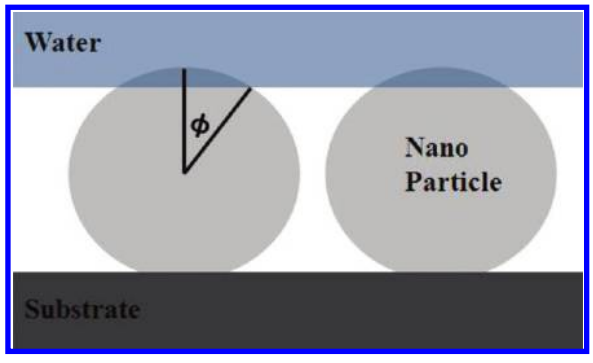

Figure 4. Schematic illustration of Cassie–Baxter nonwetting behavior on close-packed hydrophobic particles.

increase in the NP concentration in spin-coating only led to building up of a second layer of NPs, as revealed by SEM images seen in Figure 2, which did not change much of the apparent water contact angle and contact angle hysteresis.

Once the surface became superhydrophobic, it was difficult to measure the receding contact angle as the water droplet tended to stick to the goniometer needle rather than the substrate. To confirm the superhydrophobicity and low flow resistance of the surface, we measured water droplet roll-off angle, which is defined as the tilt angle when the liquid drop starts to move on a surface. A very small tilt angle (less than 5°) was observed on all superhydrophobic surfaces.

The spacing between the rough textures is important to the wetting/nonwetting behaviors. It has been shown that increasing the distance between microposts increases the receding contact angles up to a certain point, followed by a decrease of the receding contact angle.[7,37] This can be explained by the increase of the solid–liquid contact, thereby increases the contact angle hysteresis. Likewise, when NPs are far apart on the substrate, water can impregnate between the NPs and becomes pinned on the exposed hydrophilic substrate, leading to large contact angle hysteresis even though the advancing water contact angle is high. When the coverage of hydrophobic particles is increased and begin to form the second layers (see inset of Figure 2d), even if the second layer is not perfectly close-packed, the underlying substrate will no longer be in direct contact with water, leaving air trapped between and

underneath the particles to achieve highly mobile contact line at the NP−air−water interface.

To support our hypothesis on the effect of packing density of F-SiO_2 NPs to nonwettability, we performed dip-coating of 0.8 wt % F-SiO_2 NP in decafluoropentane on TESPSA treated Si. The advancing water contact angle was 88.9 ± 2° (see Table 1, sample 6) with contact angle hysteresis of ~30°, which was in sharp contrast to an advancing water contact angle of 160.4 ± 2° and nonmeasurable receding water contact angle from the spin-coated sample of the same NP concentration. SEM images confirmed the difference in surface coverage of F-SiO_2 NPs: whereas the spin-coated NPs (Figure 2c) were nearly close-packed to cover the whole surface, the dip-coated NPs (Figure 5) were loosely deposited on the substrate, and the surface coverage was even lower than that of spin-coated film from 0.1 wt % NPs (see Figure 2a). Consistent with the low surface coverage, the dip-coated film from 0.8 wt % NP solution showed smaller water contact angle than that of 0.1 wt % spin-coated NP film. In general, we observed that the packing density of F-SiO_2 NPs from spin-coating were much higher than that from dip-coating. This may be explained by the relatively poor wettability of F-SiO_2 NP/decafluoropentane solution on TESPSA treated, hydrophilic Si when dip-coating the NPs. In the case of spin-coating, however, the high shear force could overcome surface effect, forcing more NPs to pack on TESPSA-treated Si.

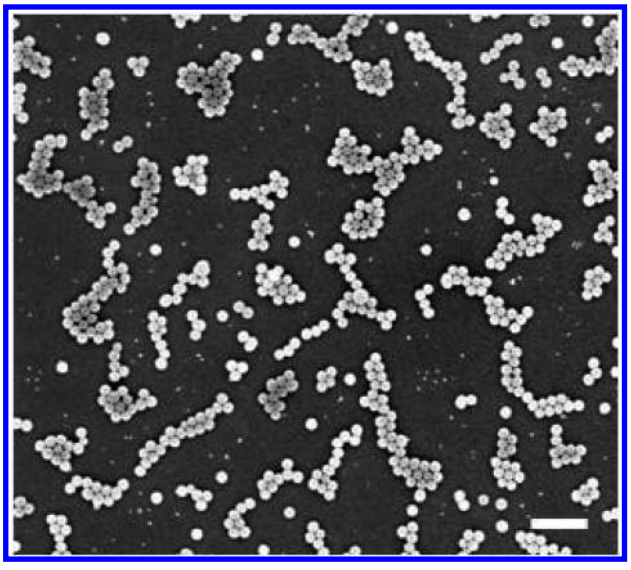

Figure 5. SEM image of F-SiO_2 NPs (0.8 wt % in decafluoropentane) dip-coated on TESPSA treated Si. Scale bar: 500 nm.

To further confirm that the exposed hydrophilic substrate, because of the loosely packed NPs, is the main reason for decreased water contact angle and increased contact angle hysteresis, we dip-coated F-SiO_2 NPs (0.8 wt %) on a hydrophobic surface, F-silane-treated Si (θ_{adv} = 113.4 ± 1°, θ_{rec} = 110.5 ± 1°). The water contact angle was found significantly increased while the contact angle hysteresis was decreased: θ_{adv} = 141.0 ± 1° and θ_{rec} = 134.1 ± 1° (Table 1, sample 7), in comparison to θ_{adv} = 88.9 ± 2° and θ_{rec} = 58.2 ± 1° from the hydrophilic, TESPSA treated Si (Table 1, sample 6).

Besides achieving superhydrophobicity without any post-treatment steps, the spin coated F-SiO_2 NP film was highly transparent: the underlying text can be clearly seen through the NP coated glass (see Figure 6a). The high optical transparency was further supported by the UV−vis spectra. Compared to the unmodified glass, F-SiO_2 NP-coated glass showed greater than 95% transmittance in the visible region (Figure 6b). The coated glass had slightly higher transmittance than the unmodified one at the near IR wavelength because of the lower refractive index contrast at the air−film interface after NP coating.

To investigate the stability of F-SiO_2 NP coating, we spin-coated 0.8 wt % F-SiO_2 NPs on glass without pre- or post-treatment and performed the water drop test and Scotch tape test. The DI water contact remained high (θ_{adv} = 148.3 ± 1°) after the drop test, although the hysteresis increased to 11.5 ± 2° (see Table S1 in the Supporting Information), implying some particles might be removed. In comparison, water contact angle was significantly decreased to θ_{adv} = 75.5 ± 2° after the Scotch tape peeling and the contact angle hysteresis was increased to 28.3 ± 2°. AFM images (see Figure S1 in the Supporting Information) showed that some NPs were removed, leaving a few pinholes after the water drop test, whereas most F-SiO_2 NPs were removed after peeling test, in agreement with contact angle measurement. These results indicate the coating is relatively robust when simply rinsed by water. However, without pre- and post-treatment of the substrate, the adhesion between NPs and glass is not sufficient

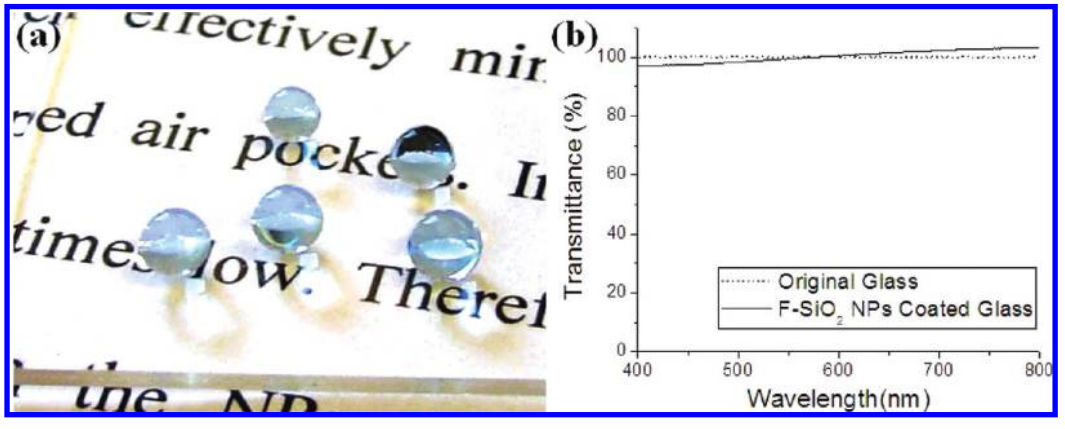

Figure 6. Optical transparency of spin-coated F-SiO_2 NP film (1.0 wt %) on a glass substrate. (a) Photograph of water droplets on F-SiO_2 NP-coated glass substrate. (b) UV−vis spectrum of the glass substrates with and without F-SiO_2 NP coating. A small amount of dimethyl methylene blue dye was dissolved in water for illustration purpose.

to sustain stronger mechanical force such as peeling and scratch.

To complete the study, we tested the possibility of creating superhydrophobic coatings on polymeric substrates, such as poly(methyl methacrylate) (PMMA) and polyester fabric. On these surfaces, oxygen plasma and vapor deposition of a hydrophobic passivation layer (e.g., fluorosilane) are not desirable. After simply spin-coating the 100 nm F-SiO_2 NPs (1.0 wt %) on these substrates, we found the surface became superhydrophobic. For example, F-SiO_2 NP-coated polyester fabric (Figure 7) has $\theta_{adv} = 160.5 \pm 2°$ in contrast to $\theta_{adv} = 92.5 \pm 1°$ from the unmodified one.

Figure 7. Optical photographs of water droplets (>10 μL) on F-SiO_2 NP-coated polyester fabric. A small amount of dimethyl methylene blue dye was dissolved in water for illustration purpose.

CONCLUSIONS

In summary, we reported a simple procedure to create a superhydrophobic surface by spin-coating fluorosilane-functionalized silica NPs without any post-treatment of the substrate with a low-surface-energy coating. The method is simple and versatile; superhydrophobicity is achieved on Si wafer, glass substrate, PMMA, and polyester fabric. SEM and AFM images indicate that at above a critical concentration, the 100 nm F-SiO_2 NPs form a nearly close-packed assembly, thus, providing the necessary surface roughness yet with minimal exposure of bare substrate. In contrast, films obtained from dip-coating have lower surface coverage of fluorosilane-functionalized SiO_2 NPs, thus, exposing the substrate in the noncovered regions. The demonstrated one-step coating method is especially attractive for user-friendly applications and for substrates that pre- and post-treatment is not desirable. The coating method can be readily extended to large surface areas and a wide range of substrates. We note, however, to create a robust, transparent superhydrophobic surface, adhesion between the hydrophobic NPs and the substrate needs to be improved.

ASSOCIATED CONTENT

Supporting Information

Additional figure and table (PDF). This material is available free of charge via the Internet at http://pubs.acs.org.

AUTHOR INFORMATION

Corresponding Author

*E-mail: shuyang@seas.upenn.edu.

Author Contributions

†These authors contributed equally to this work.

Notes

The authors declare no competing financial interest.

ACKNOWLEDGMENTS

The project is supported by NSF CAREER award, DMR-0548070. Penn Regional Nanotech facility and The Nano-Bio Interface Center (NBIC) are acknowledged for access SEM and AFM, respectively. We thank Nissan Chemical for providing SiO_2 NPs, 3M for providing fluorinated solvent, and Bigsky Technologies for providing polyester fabric.

REFERENCES

(1) Shibuichi, S.; Onda, T.; Satoh, N.; Tsujii, K. *J. Phys. Chem.* **1996**, *100*, 19512.
(2) Bico, J.; Tordeux, C.; Quéré, D. *Europhys. Lett.* **2001**, *55*, 214.
(3) Bico, J.; Thiele, U.; Quéré, D. *Colloids Surf., A* **2002**, *206*, 41.
(4) Gao, L. C.; McCarthy, T. J. *Langmuir* **2009**, *25*, 14105.
(5) Onda, T.; Shibuichi, S.; Satoh, N.; Tsujii, K. *Langmuir* **1996**, *12*, 2125.
(6) Chen, W.; Fadeev, A. Y.; Hsieh, M. C.; Oner, D.; Youngblood, J.; McCarthy, T. J. *Langmuir* **1999**, *15*, 3395.
(7) Öner, D.; McCarthy, T. J. *Langmuir* **2000**, *16*, 7777.
(8) Nakajima, A.; Hashimoto, K.; Watanabe, T.; Takai, K.; Yamauchi, G.; Fujishima, A. *Langmuir* **2000**, *16*, 7044.
(9) Cottin-Bizonne, C.; Barrat, J.-l.; Bocquet, L.; Charlaix, E. *Nat. Mater.* **2003**, *2*, 237.
(10) Erbil, H. Y.; Demirel, A. L.; Avci, Y.; Mert, O. *Science* **2003**, *299*, 1377.
(11) Shiu, J. Y.; Kuo, C. W.; Chen, P. L.; Mou, C. Y. *Chem. Mater.* **2004**, *16*, 561.
(12) Han, J. T.; Lee, D. H.; Ryu, C. Y.; Cho, K. W. *J. Am. Chem. Soc.* **2004**, *126*, 4796.
(13) Krupenkin, T. N.; Taylor, J. A.; Schneider, T. M.; Yang, S. *Langmuir* **2004**, *20*, 3824.
(14) Leng, B. X.; Shao, Z. Z.; de With, G.; Ming, W. H. *Langmuir* **2009**, *25*, 2456.
(15) Tadanaga, K.; Kitamuro, K.; Matsuda, A.; Minami, T. *J.Sol–Gel Sci. Technol.* **2003**, *26*, 705.
(16) Su, C. H.; Li, J.; Geng, H. B.; Wang, Q. J.; Chen, Q. M. *Appl. Surf. Sci.* **2006**, *253*, 2633.
(17) Artus, G. R. J.; Jung, S.; Zimmermann, J.; Gautschi, H. P.; Marquardt, K.; Seeger, S. *Adv. Mater.* **2006**, *18*, 2758.
(18) Kim, M.; Kim, K.; Lee, N. Y.; Shin, K.; Kim, Y. S. *Chem. Commun.* **2007**, 2237.
(19) Bravo, J.; Zhai, L.; Wu, Z.; Cohen, R. E.; Rubner, M. F. *Langmuir* **2007**, *23*, 7293.
(20) Zimmermann, J.; Artus, G. R. J.; Seeger, S. *J. Adhes. Sci. Technol.* **2008**, *22*, 251.
(21) Li, G. X.; Liu, Y.; Wang, B.; Song, X. M.; Li, E.; Yan, H. *App. Surf. Sci.* **2008**, *254*, 5299.
(22) Steele, A.; Bayer, I.; Loth, E. *Nano Lett.* **2008**, *9*, 501.
(23) Levkin, P. A.; Svec, F.; Fréchet, J. M. J. *Adv. Funct. Mater.* **2009**, *19*, 1993.
(24) Latthe, S. S.; Imai, H.; Ganesan, V.; Kappenstein, C.; Rao, A. V. *J. Sol–Gel Sci. Technol.* **2009**, *53*, 208.
(25) Im, M.; Im, H.; Lee, J. H.; Yoon, J. B.; Choi, Y. K. *Soft Matter* **2010**, *6*, 1401.
(26) Ling, X. Y.; Phang, I. Y.; Vancso, G. J.; Huskens, J.; Reinhoudt, D. N. *Langmuir* **2009**, *25*, 3260.
(27) Karunakaran, R. G.; Lu, C.-H.; Zhang, Z.; Yang, S. *Langmuir* **2011**, *27*, 4594.

(28) Kallury, K. M. R.; Macdonald, P. M.; Thompson, M. *Langmuir* **1994**, *10*, 492.
(29) Wenzel, R. N. *Ind. Eng. Chem.* **1936**, *28*, 988.
(30) Cassie, A.; Baxter, S. *Trans. Faraday Soc.* **1944**, *40*, 546.
(31) Lin, P. C.; Yang, S. *Soft Matter* **2009**, *5*, 1011.
(32) McConnell, M. D.; Yang, S.; Composto, R. J. *Macromolecules* **2009**, *42*, 517.
(33) Wang, D. Y.; Möhwald, H. *Adv. Mater.* **2004**, *16*, 244.
(34) Jiang, P.; McFarland, M. J. *J. Am. Chem. Soc.* **2004**, *126*, 13778.
(35) Gu, Z.-Z.; Uetsuka, H.; Takahashi, K.; Nakajima, R.; Onishi, H.; Fujishima, A.; Sato, O. *Angew. Chem., Int. Ed.* **2003**, *42*, 894.
(36) Yang, H. T.; Jiang, P. *J. Colloid Interface Sci.* **2010**, *352*, 558.
(37) Bhushan, B.; Her, E. K. *Langmuir* **2010**, *26*, 8207.